Inverted conical methane/air flame shape transformation under acoustic excitation

Cite as: Phys. Fluids **33**, 053610 (2021); https://doi.org/10.1063/5.0050260
Submitted: 13 March 2021 . Accepted: 26 April 2021 . Published Online: 20 May 2021

A. I. Krikunova, K. Y. Arefyev, A. S. Saveliev, G. A. Kossov, and A. D. Cheshko

Physics of Fluids ARTICLE scitation.org/journal/phf

Inverted conical methane/air flame shape transformation under acoustic excitation

Cite as: Phys. Fluids 33, 053610 (2021); doi: 10.1063/5.0050260
Submitted: 13 March 2021 · Accepted: 26 April 2021 ·
Published Online: 20 May 2021

A. I. Krikunova,[a] K. Y. Arefyev, A. S. Saveliev, G. A. Kossov, and A. D. Cheshko

AFFILIATIONS

Moscow Institute of Physics and Technology, 9 Institutskiy per., Dolgoprudny, Moscow Region 141701, Russian Federation

[a]Author to whom correspondence should be addressed: krikunova@phystech.edu

ABSTRACT

An inverted conical plane-symmetrical premixed methane–air flame under acoustic excitation was investigated experimentally. The flame was a conical one stabilized by a thin transverse rod. The Reynolds numbers were varied within 400–3000, and the fuel equivalence ratios were 0.8–1.4. Such a flame can take the shape of two fundamentally different types: M—when the flame front attaches both to the nozzle edge and stabilization rod; V—only to the stabilization rod. The transition conditions from one front configuration to another (M–V and V–M) were studied under various excitation parameters. Acoustic disturbances with a frequency of up to 420 Hz and an amplitude of longitudinal velocity pulsations up to 10% of the mean flow velocity excited the flame. New experimental data were obtained on the conditions corresponding to the M–V and V–M transitions. Qualitative and quantitative parameters of the hysteresis effect at which M–V and V–M transitions are realized, similar to the case of swirling flames, were revealed. The frequencies at which the acoustics most strongly affects the M–V and V–M transitions conditions were found. The hysteresis deterioration for M–V and V–M transitions was shown for the first time. It was noted that the conditions for the hysteresis deterioration are close to the theoretical frequency of the descent of vortices from the nozzle edge. The local maxima of the characteristic Strouhal numbers corresponding to the features of the minimum divergence of the flow velocities at the M–V and V–M transitions were determined.

I. INTRODUCTION

Most modern power plants[1,2] and technological devices[3–5] operate based on the fuel and oxidizer combustion process. The resultant thermal energy can be used to heat structural elements or heat-transfer agent as well as perform technological operations. Over the last few years, there has been increasing interest in clean combustion (low NO_x emissions).[6] Premixed flames application is the most environmentally friendly combustion method. There are no zones with partially unreacted components due to the uniform fuel-to-oxidizer ratio and, therefore, the emissions of carbon and nitrogen oxides are minimized. Furthermore, lean premixed combustion decreases the adiabatic flame temperature and consequently reduces the NO_x emission production rate.[7] The comparative simplicity of premixed combustion mode organization also contributes to its widespread implementation.

Methane is one of the priority types of hydrocarbon fuel in terms of improving the devices' environmental friendliness that uses fossil fuel energy and allows a significant reduction of deposits and soot formation due to the absence of heavy fractions.[8] Methane application makes it possible to reduce NO_x emission and increase the power propulsion system's thermal efficiency due to operation in lean combustion modes.[9,10] However, the effective use of methane, especially in combination with air as an oxidizer agent, requires solving some fundamental problems, namely, relatively narrow flammability limit range, long ignition delay time, low burning velocity, and the detonation possibility.[11–17]

In this manner, improvement of power propulsion systems and technological devices is closely related to improvement of the combustion process efficiency. It requires solving such important scientific problems as flame front stabilization and combustion process intensification. The vortex zones organization[18–20] behind special niches, steps, or various geometry bluff bodies (stabilizers) is one of the most widely used methods of premixed flame stabilization, especially at high speed. Residence time sufficient for chemical reactions is realized in the formed vortex zones, and the stabilizers themselves are usually heated up to high temperature, which ensures combustion stabilization. Stable and near-blowoff combustion modes, including flames stabilized by bluff bodies, are often the subject of modern scientific research.[21–25] However, velocity pulsations in vortex structures can initiate significant heat release fluctuations leading to combustion instabilities and even, under certain conditions, to flame

extinction.[26–28] Furthermore, thermoacoustic instabilities suppression is one of the major challenges in modern stationary power-plants design.[29–32] These instabilities are a nonlinear effect resulting from the interaction of unsteady heat release, acoustics, and hydrodynamics. They lead to high-amplitude pressure, flow field, and flame oscillations, and therefore, they are an unfavorable factor for industrial power installations. The combustion instabilities prediction requires the appropriate models that describe the corresponding flame and external disturbances coupling. However, acoustics can lead to a decrease in NO_x emissions for the lean premixed flames.[33] Flame shape and its stability are some of the most important criteria of the operation process quality.

Model flames are often used in laboratory research. The most common premixed flame model is a conical one.[34,35] And a thin rod is one of the options for bluff body stabilization, which leads to the vortex zones formation both behind the stabilizer and above the nozzle edge. In this case, an inverted conical flame is produced, which has significantly greater stability than a conical one.[36] It can be of two types: axisymmetric and plane-symmetric. A central rod is used for axisymmetric flame and a transverse rod—for plane-symmetric one. Such flame can take the form of M and V depending on the set of parameters: flow rate, equivalence ratio, and gravity conditions. The stability of plane-symmetrical methane–air flame was shown previously by the author.[37] The flame takes an M-shaped form—the flame front is stabilized both in a bluff body vortex zone and in a nozzle thin rim vortex zone. Alternatively, if the flame front stabilizes only in a bluff body vortex zone, a V-shaped flame is observed. Most commonly, previously studied flames with a similar flow configuration were considered as two flame front branches (V-shaped flame).[38] The concept of flame front stabilization in the vicinity of both vortex zones (M-shaped flame) was insufficiently studied. That way, the transition from M to V flame shape was studied in Ref. 39. However, the M-shaped flame was considered as the flame, where front branches are bent down and do not attach to the nozzle edge. Even though the M-shaped flame exists under low flow rates, its research is important for a deeper understanding of the combustion nature. For example, in Ref. 25, the dynamics of a plane-symmetric inverted conical flame under the near-blowoff and immediately upon blowoff was investigated. The dynamics of interacting flames in rectangular-slot burners was studied in Ref. 40, where the transition from one flame shape to another one (similar shapes M, V, as well as more diverse ones) was reported. Partly the current issue was considered in Ref. 41: a flame stabilized by a vertical thin rod at a certain flow rate and equivalence ratio take the M shape. Similarly, the M and V flame modes can be realized when the flow swirls in the combustion chambers depending on the flow parameters.[41–44] It was shown that the transition between such combustion modes is ambiguous both in the case of swirling[41] and during stabilization by the transverse cylinder.[37] Flames exhibit different stability depending on the shape.[45] The issue of stability and other characteristics of rod-stabilized flames are also studied numerically.[46–49] Besides, the above type of flame is widely studied from the point of view of the turbulence effect on the flame front structure,[50] including the interaction of coherent structures and stochastic fluctuations.[51]

The acoustic forcing mechanisms for laminar premixed C-, V-, and M-flames have been studied by different scientific groups.[52–55] Premixed flame and acoustics interaction was considered based on a linearization of the G-equation for an inclined flame including convective effects of the flow modulations propagating upstream the flame in Ref. 53. Transfer functions comparison for conical and inverted conical flames (stabilized by a central rod) showed that V-shaped flames are more responsive to external disturbances than conical ones. It was reported that the V-flame response strongly depends on fluctuations amplitude even for moderate perturbation levels. Furthermore, it was shown that the flame front shape plays a key role in the response of combustion to external acoustic perturbations.[54] Also, the V-flame dynamics is controlled by the roll-up of the flame front around the vortices shed in the shear layer established between the fresh stream and the surrounding air. Blowoff characteristics (stability parameters) of the inverted conical flame under acoustic excitation were investigated earlier.[24]

Considering the above, the study of premixed methane–air flame features is an important stage in fundamental research to improve the operating process quality in power propulsion systems and technological devices. At the same time, despite numerous studies of reacting flows and acoustics coupling, not all aspects of this issue have been fully studied. In the present work, the problem of premixed bluff-body stabilized methane–air flame stability under the acoustic disturbances in the conditions of normal gravity was considered. The work is devoted to the analysis of inverted conical flame shape changes (M–V and V–M transitions). This issue has not been previously studied in the literature.

II. EXPERIMENTAL DETAILS

The experimental setup used in the present study is shown in Fig. 1. It consists of a cylindrical mixing chamber (1) with an inner diameter of 30 mm and a length of 1.2 m; on one side of which a nozzle (burner, 2) is installed with an outlet diameter of 15 mm and a length of 0.17 m and on the other side an acoustic pulsator is connected. The total height of the installation is 2.12 m. The pulsator is a metal confuser (4) with a maximum diameter of 300 mm, the outlet section of which is 30 mm. Inside the pulsator, there is a GD25 type loudspeaker (5) with a resistance of 4 Ohms and a diffuser (6) with a diameter of 250 mm. The volume near the bottom of the pulsator cup and the volume near the outlet section of the confuser are connected by a tube (11) with an inner diameter of 8 mm in order to ensure free flow of air between the sides of the loudspeaker cone. Excitation of loudspeaker cone oscillations is provided by power amplifier LV103 with a maximum output power 100 W (13). The excitation of fixed frequency harmonic oscillations is initiated by a digital generator (14) Rigol DG4062, the output signal of which is fed to the input of the power amplifier. The output signal voltage amplitude of the power amplifier is controlled using a digital oscilloscope (17) Rigol DS1054Z, which registers the amplitude of the amplifier output signal (Vpp, peak-to-peak voltage). The pulsator and the mixing chamber are isolated from each other by an elastic membrane (6) made of latex. This is done for two reasons, one of which is to prevent the accumulation of a combustible mixture inside the pulsator for safety during the experiment. The second reason is to prevent an intensive gas movement inside the mixing chamber, which can significantly distort the velocity profile at the nozzle outlet section. That could occur due to the significant amplitude (up to 1 cm) of the diffuser movement, as well as due to the significant difference in the cross-sectional area of the loudspeaker diffuser and the internal section of the mixing chamber (the ratio of these areas is about 70). At a relatively low frequency

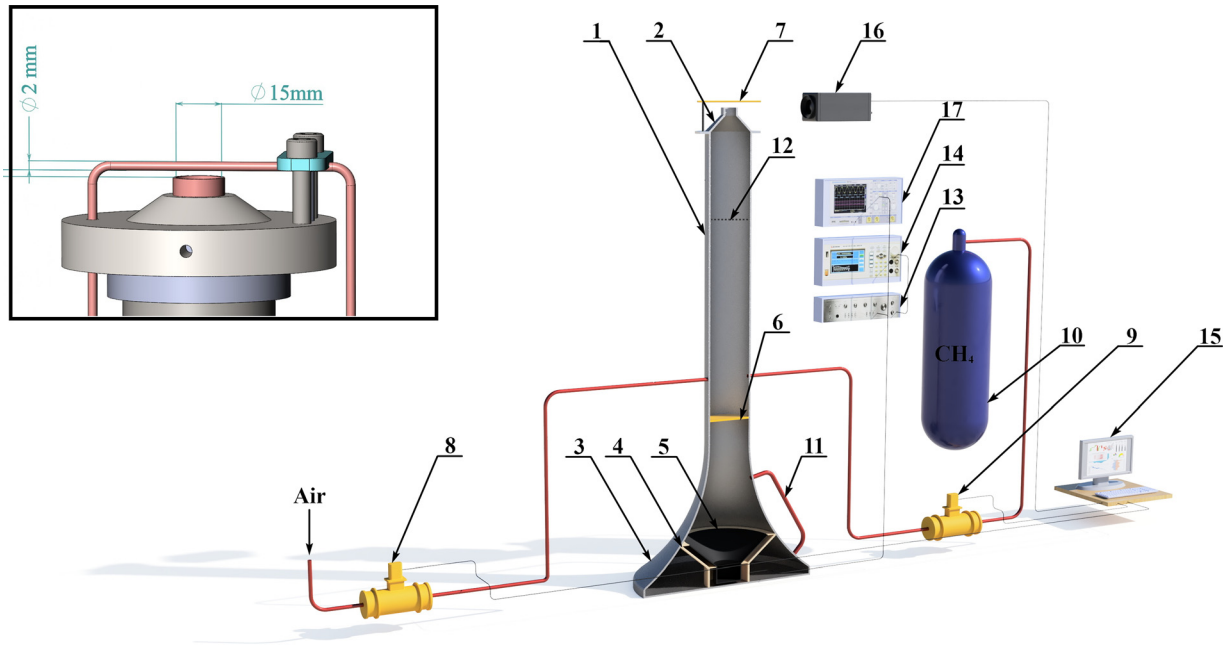

FIG. 1. The experimental setup scheme: 1—mixing chamber, 2—nozzle (burner), 3—contraction cone, 4—convergent tube, 5—loudspeaker, 6—membrane, 7—stabilizer, 8—air flow meter, 9—methane flow meter, 10—methane tank, 11—bypass tube, 12—metal mesh, 13—amplifier, 14—signal generator, 15—computer, 16—video camera, and 17—oscilloscope.

of sound excitation (of the order of 10 Hz) at the amplifier maximum output power, the membrane oscillations amplitude is of the order of 1 cm, whereas at a high frequency (of the order of 100 Hz), this amplitude is of the order of 1 mm.

Dry air and methane (99.99% purity) are fed into the mixer near the upper side of the membrane. The gases are supplied in an opposite way, so that they mix with each other, passing the distance from the membrane to the nozzle outlet section. A flame arrester (a metal mesh 12) is installed between the mixer (1) and the nozzle (2) in order to prevent flame flashback inside the rig. The Bronkhorst flow meters (8 and 9) are used to set and measure the air and methane flow rate using a control program developed by the authors. The program specified the flow velocity (Reynolds number) and the fuel equivalence ratio φ (the ratio of the molar fraction of methane in the combustible mixture to the molar fraction of methane in the stoichiometric combustible mixture). Based on that data, the program automatically calculates the required air and methane mass rate. Mean flow velocity was varied in range 0.4–3.5 m/s, which belonged to laminar combustion without acoustic excitation; the mixture equivalence ratio was varied in the range 0.8–1.4. The program also has the ability to control the flow rate deviation from the set value. Additionally, the program provides for the possibility of a gradual flow rate increase (decrease) at a constant equivalence ratio; this feature was used to study flow parameters of the M–V and V–M flame front transition. The experiments were carried out at room temperature and atmospheric pressure. In order to obtain an inverted conical flame, a thin steel cylindrical rod (7) as a bluff-body was used. A stabilizer has a diameter of 2 mm (its diameter was controlled with a micrometer) and a length of 10 cm, significantly exceeding the burner's outlet section. The stabilizer was rigidly mounted on a special pedestal so that any displacement relative to the nozzle outlet section was excluded. The axis of the stabilizer was located at a distance of 4 mm from the plane of the nozzle exit section and parallel to it. The bluff-body allows expanding the flame stability in comparison with conical flame. When the flame blowoff from nozzle edges, it continues to be anchored to the rod (existing in the form of a V-shaped flame). In this case, the resulting flame (type M or V) was symmetric with respect to the plane that passes through the axis of the stabilizer and the nozzle axis. The flame shape was recorded on a PC (15) using a video camera (16), and the lens optical axis of which coincided with the stabilizer axis. Mean flow rate u_{mean} and fuel equivalence ratio φ were registered for the moment of transition from one flame shape to another one (from M to V or from V to M). Flame images of typical conical, M, and V shapes are shown in Fig. 2.

Registration on the transition parameters proceeded as follows. Combustible mixture ignition was carried out under conditions of methane and air flow rate that guarantee stable combustion for all excitation levels: flow velocity $u_{mean} = 1.0$ m/s and $\varphi = 1.0$. After stable combustion establishment, the fuel equivalence ratio was changed to the desired value. If M-flame was observed, then the procedure for evaluating the parameters of the M–V transition was carried out, otherwise, of the V–M transition. Keeping the fuel equivalence ratio constant, the methane and air flow rates were changed in such a way that the outlet section velocity increased/decreased step by step 0.01 m/s every 10 s. In the present study, the flame was considered to have completed an M–V transition, when the flame front branches detached from the nozzle edge and rose upward. At this moment, the flow rate value and fuel equivalence ratio for the M–V transition were recorded. The flame front branches moved upstream with the subsequent bend

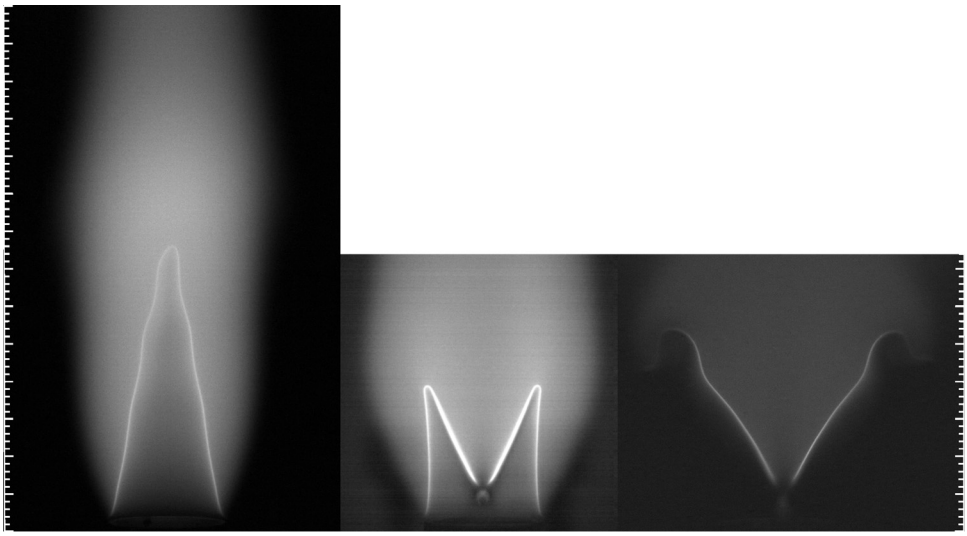

FIG. 2. Typical images of the flame chemiluminescence for Re = 2000, $\varphi = 1.2$: conical flame, M-shaped one and V-shaped one.

and attachment to the nozzle edge under the flow velocity decrease. At this moment, the conditions of the V–M transition were recorded. The described sequence of operations was performed for different values of the fuel equivalence ratio. As a result, the graphs of the flow rate vs fuel equivalence ratio for the M–V and V–M transitions were obtained. Also, such transition conditions were studied under acoustic perturbations. The experiments were repeated at given values of the excitation frequency f (from 10 to 420 Hz) and the value of the relative velocity fluctuations $\frac{u'}{u_{mean}}$ (from 0%, i.e., without acoustics, up to 10%). The flame stability was estimated at a constant acoustic amplitude in each series of experiments for universalization and generalization of the results, since this is made possible to evaluate the features of the flame behavior without taking into account the features of the setup amplitude–frequency response.

III. ACOUSTIC CHARACTERISTICS OF EXPERIMENTAL SYSTEM

The flow parameters for flame shape transition were estimated at constant levels of velocity fluctuations. For this purpose, preliminary experiments were carried out. Levels of velocity fluctuations u', corresponding to the amplitude of the voltage Vpp applied to the speaker, were determined using the Dantec miniCTA hot-wire anemometer complex at a given frequency f. Hot-wire sensor 55P11 was set up in a nozzle outlet cross section. The measurements were performed for the isothermal flow. The hot-wire sensor was attached using a high-accuracy (up to 0.01 mm) coordinate system. The temporal shapes of the sensor signal, as well as the outlet velocity profile, were measured. A typical waveform of the signals recorded by the hot-wire anemometer for various amplitudes of acoustic disturbances (1%, 2%, 5%, and 10%) is shown in Fig. 3. The data show the flow characteristics with Re = 3000 disturbed with f = 60 Hz. Figure 4 shows the characteristic profiles of the time-averaged velocity $u_{mean}(r)$ and velocity fluctuations $\frac{u'}{u_{mean}}(r)$ along the nozzle radius at different levels of acoustic disturbances (1%, 2%, 5%, and 10%). It can be seen that both the mean velocity profiles and the profiles of velocity fluctuations are close to rectangular for all excitation modes and without it.

By measuring and analyzing the signal of the hot-wire sensor, a function h of the form $\frac{u}{u'} = h(V_{pp}, f, u_{mean})$ was experimentally obtained, which was used to maintain a constant value of the velocity fluctuation amplitude during the experiments.

IV. RESULTS AND DISCUSSION: M–V AND V–M FLAME SHAPE TRANSITION UNDER THE VARIOUS AMPLITUDES AND FREQUENCIES

The conditions of the M–V and V–M flame shape transitions were found experimentally. The results were represented through the stability diagrams: flow velocity vs fuel equivalence ratio for M–V and

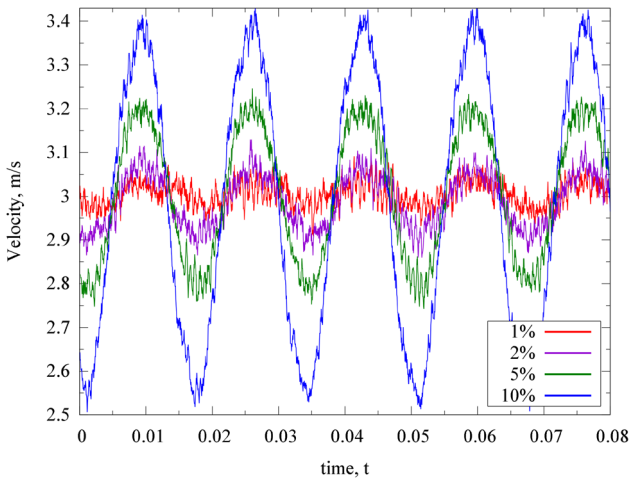

FIG. 3. Typical temporal realization of velocity with a variation of the excitation amplitude.

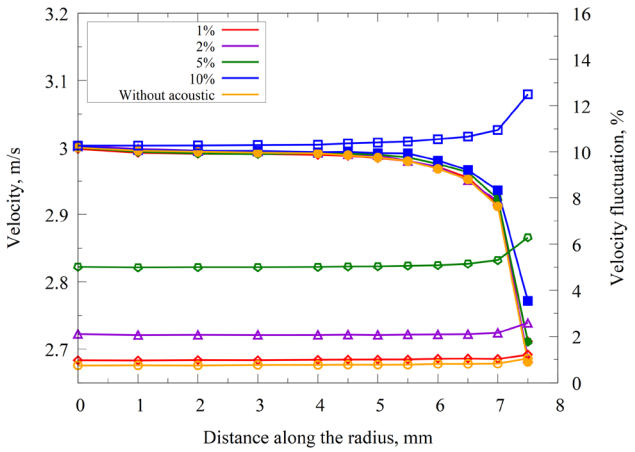

FIG. 4. Typical profiles of the time-averaged velocity $u_{mean}(r)$ (closed signs) and velocity fluctuations $\frac{u'}{u_{mean}}(r)$ (open signs) along the nozzle radius.

V–M flame shape transitions. The results at various parameters of acoustic impact (frequency, amplitude) are represented in Fig. 5. It is shown that transition conditions have the property of hysteresis. In other words, the conditions of the M–V and V–M transitions at a constant fuel equivalence ratio differ in flow velocity. For example, flame ignited at u = 1.5 m/s and $\varphi = 0.9$ has V-shape. The flow velocity gradual decrease under constant fuel/oxidizer ratio brings to the flame shape change to M-configuration under flow velocity equals to 0.86 m/s. Consequent velocity increase brings to the V-flame under conditions u = 1.31 m/s. The similar processes occur for other fuel equivalence ratios and excitation conditions.

A similar hysteresis effect is usually observed in swirling flames.[56–58] Often, such phenomena were observed in the presence of a wall near the flame (combustion chambers). The hysteresis in such conditions is significantly affected by heat transfer with combustor walls. Thereby, it is important to consider non-adiabatic boundary conditions and their effect on the reaction rate.

In the experiments under discussion, M–V and V–M flame front transitions represent the blow-off and attachment of the flame front at the nozzle edge. In this case, the flame remains stabilized in the vortex zone behind the cylindrical stabilizer. The results concerning conical flame stability (the flame is stabilized only by the burner thin edge) also are represented in the current work. From the point of view of the action mechanisms, M–V and V–M transformations should be distinguished. Such transitions differ, among other things, in a set of factors taken into account in the stabilization process. Considering the stability issue from this angle, it can be said that flame front stretching plays an important role in the M–V transition. Also, blow-off and attachment modes for rich and lean mixtures should be considered separately. The vorticity field changes under acoustics, which leads to an increase in the diffusion of the external oxidizer into the combustion region. In the case of rich flames, such process leads to a greater dilution of the mixture with oxidizer and, consequently, an approach to the stoichiometric mixture in the combustion region.

A. Blow-off/attachment from the nozzle edge

Such a transition must be considered from the point of view of the shear layer flame stabilization physics. In this case, two key physical processes play a role: flame front stretching and recirculation zone deformation. Acoustics affects all of the above processes. For example, the front stretch introduced by the shear layer can be estimated as $k_{s\,shear} = S_L\left(\frac{u_0}{L_{shear}\vartheta}\right)^{1/2}$ where S_L—is the flame front propagation speed, u_0—is the flow rate, L_{shear}—is the shear layer thickness, ϑ—is the kinematic viscosity.[59] Consequently, the acoustic field introduces a periodic increase in the flow velocity u_0, which leads to an increase in the flame front stretching and stability decrease, which was observed in all experiments under discussions. Low-intensity acoustics at any frequencies does not introduce noticeable changes in the flow velocity (pulsations are at the level of turbulent fluctuations). Such

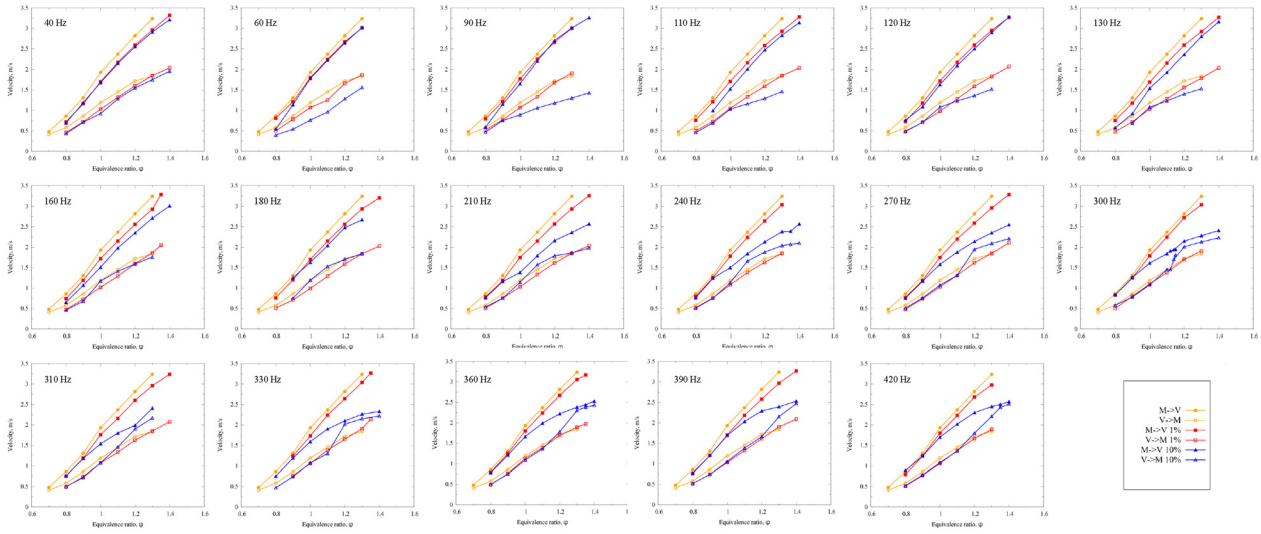

FIG. 5. Diagrams of flame stability under acoustic excitation: conditions of flow velocity under M–V and V–M flame shape transitions vs fuel equivalence ratio.

disturbances slightly changes flame stability, both in the case of lean mixtures and in the case of rich ones. Figure 6 shows the conditions of the inverted conical flame M–V transitions and the conical flame blow-off. It can be seen that without disturbance and at low excitation amplitudes (1%) the boundaries coincide. The results are presented both for relatively low excitation frequencies—60 Hz, and for sufficiently high—300 Hz. Hence, the statement that the steady-state flow structure plays an important role in the nature of the response of the combustion process to velocity fluctuations given in Ref. 54 cannot be applied in the entire excitation region, whereas with a disturbance amplitude increase, the response of the flame depends on the excitation frequency. In this case, the response of the conical and inverted conical flame is similar. It is also worth noting the difference between the response of lean and rich mixtures. The flow velocity increase for the transition conditions is observed within a fuel equivalence ratio increase.

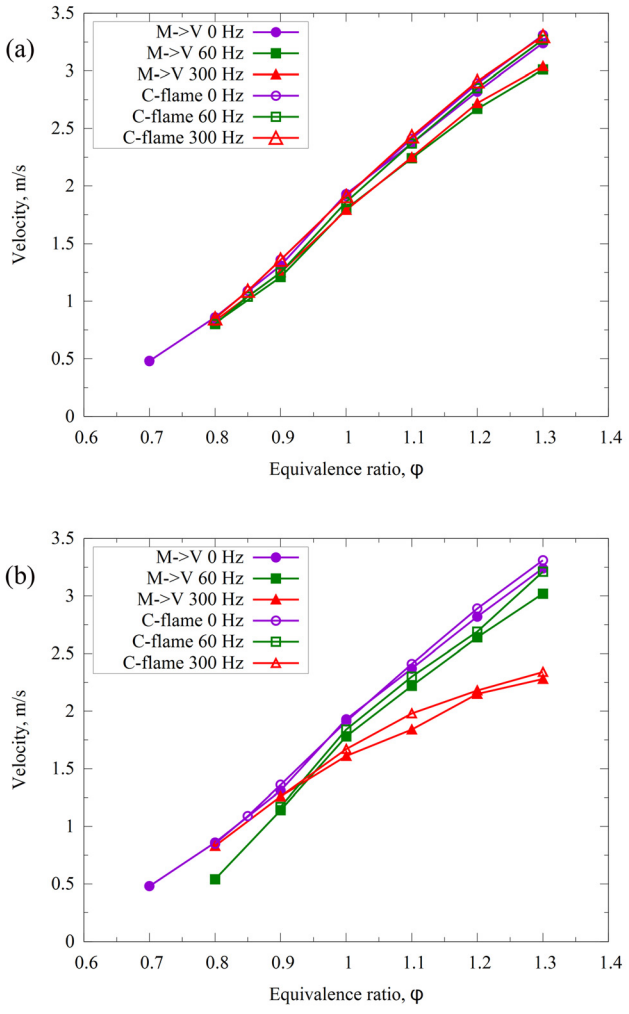

FIG. 6. Comparison of conical flame blowoff conditions (C-flame blow-off) and conditions for the M–V inverted conical flame shape transition (M–V transition) excited by various frequencies and amplitudes: (a) 1% and (b) 10%.

Similar to Ref. 53, it was found that the M-flame can also be an amplifier of acoustic disturbance. The greatest amplification was observed at the moment immediately preceding the M–V transition. After the transition, the noise intensity (of the V-shaped flame) drops sharply at the same level of acoustic excitation.

B. Hysteresis effect

For lean flames, it can be considered the linear dependence between flow rate (Reynolds number) and fuel equivalence ratio (stability curve) both for M–V and V–M transitions for all frequencies under consideration. Typical linear dependences of the flow rate vs fuel equivalence ratio under the conditions of the transition from one flame-shape to another one under acoustic excitation of 160 Hz and 10% are shown in Fig. 7(a). It can be seen that the relation can be approximated by linear functions with a slope marked with one of the Greek symbols in Fig. 7. The conditions for the M–V transition for lean flames ($\varphi \leq 1$) are represented by the angle of inclination α, rich ones ($\varphi > 1$)—ß, the conditions for the V–M transition for lean flames ($\varphi \leq 1$)—γ, rich ones—ζ. For rich flames, the dependences (stability curve) can be regarded as linear only up to a specified frequency 160 Hz. For high frequencies, the dependences can be successfully approximated by polynomials up to the third order. A slower increase in the transition flow rate under mixture enrichment is observed at these frequencies. Thus, it is convenient to consider the behavior of the flame by analyzing the slope of the lines mentioned above (the dimensional ratio of the flow velocity and the fuel equivalence ratio). The results for all frequencies of a constant amplitude of 10% are shown in Fig. 7(b).

For lean flames (green and blue), it can be observed that the hysteresis region narrows under the excitation frequency increase up to a critical frequency of 160 Hz. This frequency will be named the first critical frequency $f_1^* = 160$ Hz. An excitation frequency increase brings to the decrease in the flow velocity under M–V transformation and the increase in the flow velocity under V–M transformation. In other words, the transition boundaries on the graph move toward each other (approach each other). Above the critical frequencies, the transition conditions are observed to be independent of the exciting frequency [the slope angle in Fig. 7(b) remains constant] both for the M–V transition and for the V–M transition. In this case, for the V–M transformation, the transition conditions remain close to the ones in the absence of disturbances. And for M–V, similar fuel equivalence ratios correspond to lower flow rates.

Rich methane–air flames excited below the first critical frequency (160 Hz) exhibit M–V transition under the same conditions as non-excited flames [almost horizontal violet line in Fig. 7(b)]. Above this frequency, both M–V and V–M transition curves in the stability diagram become substantially nonlinear. Therefore, there are no data concerning the rich flames for the frequency range above the critical value in Fig. 7(b). For the V–M transition, the flow velocity with increasing frequency has a variable tendency. Below the 160 Hz excitation, the V–M transition occurs at a lower flow rate in comparison with the non-excited flame. For the disturbance with frequency above 160 Hz, the V–M transition occurs at a higher flow rate in comparison with the non-excited flame. The stability (transition conditions) change can be explained as follows: with an excitation increase the diffusion of the oxidant into the combustion zone increases, which in its term increases the stability, since the mixture in a combustion zone

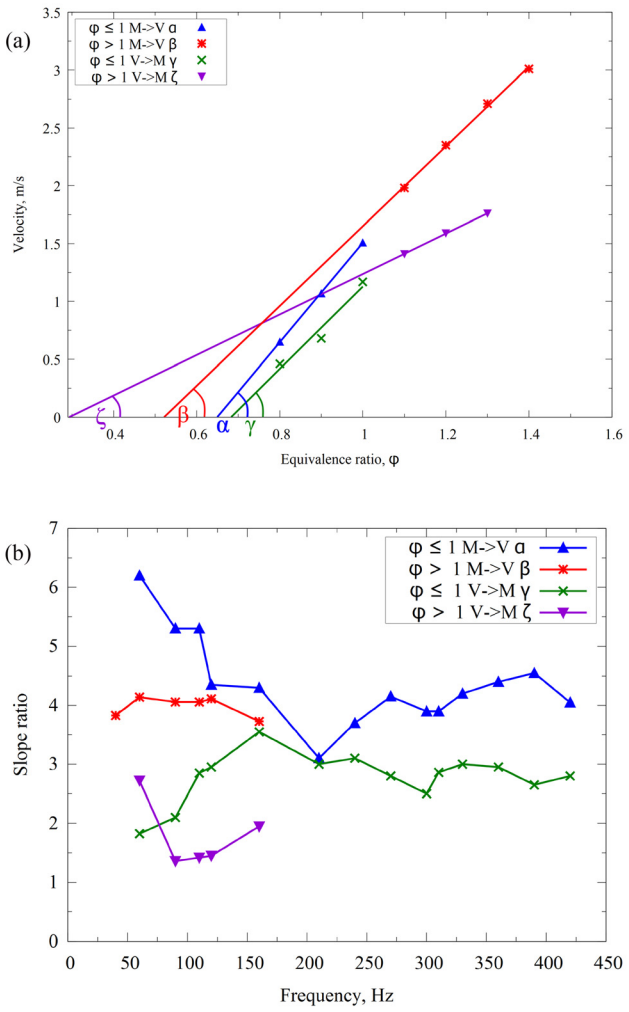

FIG. 7. (a) A typical stability curves and slopes determination; (b) The slopes of the stability curve versus the excitation frequency.

approaches a stoichiometric one. At further frequency increase, the effect of acoustic intensification of heat transfer begins to prevail, which leads to the removal of energy from the reaction zone, as result, the flame temperature drops and, therefore, its stability decreases. This process intensifies with a frequency increase. In other words, at low "subcritical" frequencies, both for lean and rich mixtures the flame behaves in the same way: the flow rate under transition increases with increasing concentration of the fuel and decreases with increasing frequency.

For each frequency, starting from a specified (critical) one, there is such a fuel/oxidizer ratio, where the hysteresis practically deteriorates. M–V and V–M transitions occur at the same combinations of flow rate and fuel equivalence ratio. To analyze such feature points, the data were treated as follows. The relative difference in the flow rates for M–V and V–M transitions was estimated $\Delta u = (u_{M\to V} - u_{V\to M})/u_{M\to V}$ for all frequencies and fuel/oxidizer ratio under consideration. For each frequency, the minimum value $\Delta u^* = min[\Delta u]$

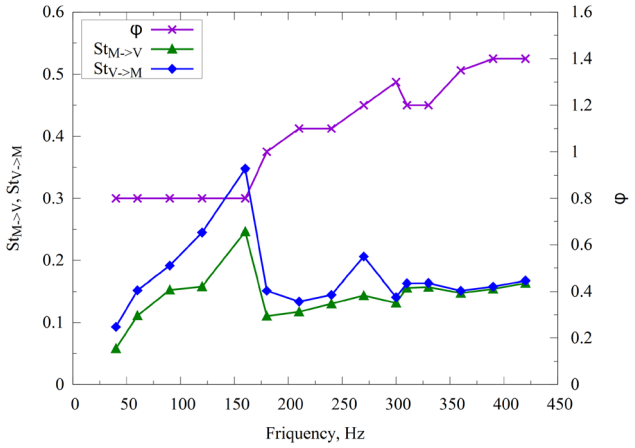

FIG. 8. Conditions for the occurrence of hysteresis degeneration.

and the corresponding minimum $\varphi = \varphi^*$ were found. The results are shown in Fig. 8 (right axis). At low frequencies, the constancy of $\varphi^* = 0.8$ is observed, which corresponds to the minimum fuel equivalence ratio in the experiments (the flame flash-back occurred below this value). The value $\Delta u^* \approx 40\%$ corresponds to that conditions. Starting from a value of 160 Hz, on the one hand, a φ^* increase is observed and, on the other hand, a sharp decrease in the value of $\Delta u^* < 20\%$. This indicates the occurrence of points of hysteresis deterioration (degeneration). For such conditions, the Strouhal number can be estimated based on the outlet nozzle diameter d, which plays the role of a stabilizer, $St = fd/u_0$. As u_0, the velocity value was chosen under the conditions of the M–V and V–M transition, respectively, $St_{M\to V} = fd/u_{M\to V}$ and $St_{V\to M} = fd/u_{V\to M}$. The results are shown in Fig. 8 (left axis). These quantities behave in a similar manner. An increase in $St_{M\to V}$ and $St_{V\to M}$ is observed up to the conditions corresponding to the first critical frequency $f_1^* = 160$ Hz, after which a sharp decline is observed at 180 Hz, and a slight increase. As the frequency increases, the moment of complete coincidence occurs: $St_{V\to M} = St_{M\to V}$. This phenomenon corresponds to $\Delta u^* < 10\%$. This value can be called the second critical frequency $f_2^* = 300$ Hz.

The hysteresis degeneration can be explained as follows. Consider a V-shaped flame with a certain fuel equivalence ratio. Under a gradual flow velocity decrease (approaching the conditions of the V–M transition), the frequency of the descent of vortices from the nozzle edge changes, respectively (depends on the velocity at a constant thickness of the edge). If the frequency of the external acoustic impact coincides with the frequency of vortex descent under current conditions, vortices are intensified due to the interaction of acoustic pulsations with the shear flow zone near the nozzle edge. This process leads to the flow chaotization in the zone downstream of the nozzle edge, i.e., just where the reattachment of the flame front branches takes place. This chaotization (randomization) contributes to a vortex zone size increase, in which the stabilization of the M-shaped flame is realized, as well as to the inflow of an additional oxidizer into this area. Due to that, the moment the V-shaped flame front edge entrance into the vortex zone occurs at a higher flow velocity. Thus, the V–M transition occurs at a higher value of the flow velocity (due to an increase in

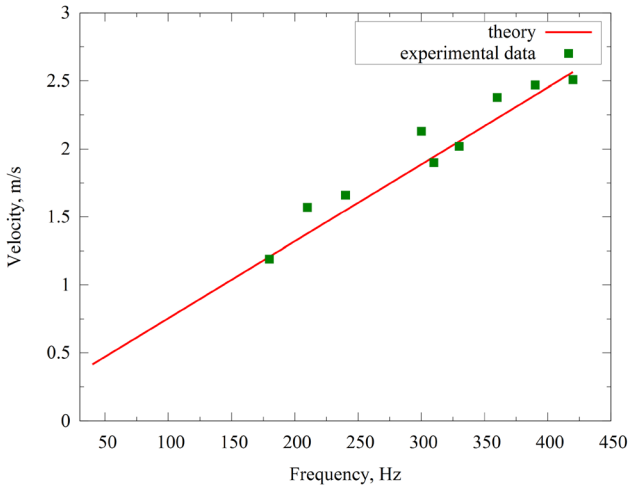

FIG. 9. Flow rate vs frequency of the vortex descent from the nozzle edge (theoretical curve) and the flow rate vs excitation frequency in the case of hysteresis deterioration (experimental data).

the vortex zone size in comparison with the case of the acoustic disturbance absence), which leads to a contraction of the region of the hysteresis effect existence.

Let us show the validity of the proposed justification. The frequency f_V of vortex generation at the edge of the burner nozzle can be estimated based on the empirical parametric dependence:[60] $St = \frac{f_V d}{u_0} = 0.212 - \frac{2.7}{Re_w}$, where $Re_w = \frac{u_0 d}{\vartheta}$—Reynolds number calculated using the wall thickness. In this case, the velocity $u_{V\to M}$ is selected as u_0 for the case of degeneration of the hysteresis. The dependence of the vortex shedding frequency on the flow velocity is shown by the red line in Fig. 9. The flow velocity value at which the V–M transition occurs for each external excitation frequency is represented by green dots. A fairly good agreement between the experimental data and the theoretical curve is observed. Therefore, it can be argued that

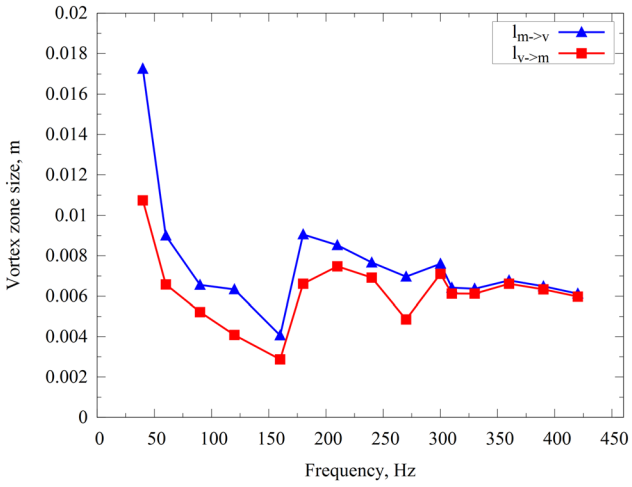

FIG. 10. Evolution of the vortex zone size above the nozzle edge depending on the acoustic excitation frequency.

this assumption is true and the degeneration of the hysteresis occurs due to the coincidence of the excitation frequency with the frequency of the vortices descent from the nozzle edge and vortices deformation.

Let us consider in somewhat more detail the issue of vorticity region deformation above the nozzle edge. The scale of the recirculation zone change under the acoustic disturbance can be estimated as $l \sim u/f$. It is legitimate to consider the flow velocity under transition in the capacity of u—$u_{V\to M}$ and $u_{M\to V}$. The results are presented in Fig. 10. A vortex zone decrease can be observed under the excitation below the first critical frequency $f_1^* = 160$ Hz. A maximum vortex zone is observed at a frequency of 180 Hz. Further disturbance frequency increase brings to the curve decline (zone decrease) but not so sharp as for the first critical frequency. Upon reaching the second critical frequency $f_2^* = 300$ Hz, the vortex zone size remains constant.

V. CONCLUSIONS

In this study, we examined the acoustics effect on the stability parameters of the inverted conical methane–air flame:

- M–V and V–M flame shape transitions under acoustic excitation, as without external disturbance, exhibit hysteresis effects.
- The conditions of the M–V transition coincide with the conditions for the conical flame blow-off, both under acoustic excitation and without external disturbance.
- Low-intensity impact (up to 1% of the mean flow rate), regardless of frequency, does not affect the transition boundaries. An intensity (amplitude) increase up to 10% brings to the noticeable effect of acoustic excitation on combustion stability.
- The acoustic impact below the first critical frequency $f_1^* = 160$ Hz for lean flames brings to the hysteresis zone contraction: the boundaries of the V–M and V–M transitions approach each other. When the exciting frequency exceeds the first critical one, the transition boundary, and, accordingly, the flame stability do not change.
- For rich mixtures, this frequency is also critical: a hysteresis deterioration takes place. For each frequency, deterioration occurs at a certain velocity/fuel equivalence ratio. This phenomenon can be explained by the coincidence of the frequencies of the vortices descent from the nozzle edge and the flame excitation frequency. The frequency of the vortex descent depends on the difference in the main flow velocity and the surrounding one. If the flame conditions are close to the unstable (transient) regime at the corresponding velocities difference, the hysteresis deterioration occurs.
- Upon reaching the second critical frequency $f_2^* = 300$ Hz, the hysteresis completely deteriorates, and the size of the vortex zone above the nozzle edge stops changing.

ACKNOWLEDGMENTS

This work was supported by the Russian Science Foundation, Grant No. 20-79-10328.

DATA AVAILABILITY

The data that support the findings of this study are available from the corresponding author upon reasonable request.

REFERENCES

[1]A. I. Lanshin and A. S. Polev, "Analysis of trends and forecast of GTE development for subsonic civil aircraft," Proceedings of the 29th Congress of the International Council of the Aeronautical Sciences (2014), Vol. 4, p. 2854.

[2]M. Banholzer, W. Vera-Tudela, C. Traxinger, M. Pfitzner, Y. Wright, and K. Boulouchos, "Numerical investigation of the flow characteristics of underexpanded methane jets," Phys. Fluids **31**(5), 056105 (2019).

[3]D. J. Wilhelm, D. R. Simbeck, A. D. Karp, and R. L. Dickenson, "Syngas production for gas-to-liquids applications: technologies, issues and outlook," Fuel Process. Technol. **71**, 139 (2001).

[4]A. V. Voronetsky, D. A. Jagodnikov, L. A. Filimonov, S. A. Suchkov, N. V. Shirjaeva, A. A. Elisseev, and E. V. Boronin, "Practical experiences with a new portable HVOF spraying and cutting system," Proceedings of the 15th International Thermal Spray Conference (1998), Vol. 2, p. 1393.

[5]C. H. Bhuvan, K. Hiranandani, B. Aravind, V. Nair, and S. Kumar, "Novel flame dynamics in rich mixture of premixed propane-air in a planar microcombustor," Phys. Fluids **32**(10), 103604 (2020).

[6]M. A. Nemitallah, A. A. Abdelhafez, and M. A. Habib, "Global Warming and Emission Regulations. In: Approaches for Clean Combustion in Gas Turbines," Fluid Mech. Its Appl. **122**, 1 (2020).

[7]V. L. Zimont, "Theory of turbulent combustion of a homogeneous fuel mixture at high reynolds numbers," Combust. Explos. Shock Waves **15**, 305 (1979).

[8]J. Urzay, "Supersonic combustion in air-breathing propulsion systems for hypersonic flight," Annu. Rev. Fluid Mech. **50**, 593 (2018).

[9]G. Tripathi, P. Sharma, and A. Dhar, "Effect of methane augmentations on engine performance and emissions," Alexandria Eng. J. **59**(1), 429 (2020).

[10]Agora Energiewende and Ember, https://static.agora-energiewende.de/fileadmin2/Projekte/2021/2020_01_EU-Annual-Review_2020/A-EW_202_Report_European-Power-Sector-2020.pdf for "The European power sector in 2020: Up-to-date analysis on the electricity transition" (2021).

[11]V. V. Azatyan, "Chain nature of the combustion, explosion, and detonation of gases: New aspects of theory," Russ. J. Phys. Chem. A **89**, 1731 (2015).

[12]N. J. Kim, "Effect of an inlet temperature disturbance on the propagation of methane-air premixed flames in small tubes," Combust. Flame **156**, 132 (2009).

[13]R. K. Cheng, "Autoignition in methane-hydrogen mixtures," Combust. Flame **58**, 125 (1984).

[14]A. A. Vasiliev, "Ignition delay in multifuel mixtures," Combust. Explos. Shock Waves **43**, 42 (2007).

[15]J. M. Austin and J. E. Shepherd, "Detonations in hydrocarbon fuel blends," Combust. Flame **132**, 73 (2003).

[16]A. A. Vasiliev, "Cell size as the main geometric parameter of multifront detonation wave," J. Propul. Power **22**, 1245 (2006).

[17]R. Hernandez-Rivera, G. Troiani, T. Pagliaroli, and A. Hernandez-Guerrero, "Detection of the thermoacoustic combustion instabilities of a slot burner based on a diagonal-wise recurrence quantification," Phys. Fluids **31**(12), 124105 (2019).

[18]M. P. Wilson, R. D. W. Bowersox, and D. D. Glawe, "Experimental investigation of the role downstream ramp on a supersonic injection plume," J. Propul. Power **15**, 432 (1999).

[19]J. P. Sislian and J. Schumacher, "Fuel/air mixing enhancement by cantilevered ramp injectors in hypersonic flows," International Symposium on Air Breathing Engines (1999).

[20]J. Wan, H. Zhao, and V. Akkerman, "Anchoring mechanisms of a holder-stabilized premixed flame in a preheated mesoscale combustor," Phys. Fluids **32**(9), 097103 (2020).

[21]A. J. Morales, I. M. Lasky, M. K. Geikie, C. A. Engelmann, and K. A. Ahmed, "Mechanisms of flame extinction and lean blowout of bluff body stabilized flames," Combust. Flame **203**, 31 (2019).

[22]Y. J. Kim, B. J. Lee, and H. G. Im, "Hydrodynamic and chemical scaling for blow-off dynamics of lean premixed flames stabilized on a meso-scale bluff-body," Proc. Combust. Inst. **37**(2), 1831 (2019).

[23]F. H. Vance, Y. Shoshin, J. A. van Oijen, and L. P. H. de Goey, "Effect of Lewis number on premixed laminar lean-limit flames stabilized on a bluff body," Proc. Combust. Inst. **37**(2), 1663 (2019).

[24]S. Chaudhuri and B. M. Cetegen, "Blowoff characteristics of bluff-body stabilized conical premixed flames with upstream spatial mixture gradients and velocity oscillations," Combust. Flame **153**(4), 616 (2008).

[25]S. Nair and T. Lieuwen, "Near-blowoff dynamics of a bluff-body stabilized flame," J. Propul. Power **23**, 421 (2007).

[26]K. Yu. Arefyev, A. I. Krikunova, and V. A. Panov, "Experimental study of premixed methane-air flame coupled with an external acoustic field," J. Phys.: Conf. Ser. **1**, 1147 (2019).

[27]K. Yu. Arefyev, A. I. Krikunova, and V. A. Panov, "Complex effect of electric and acoustic fields on air-methane flame blow-off characteristics," High Temp. **57**, 909 (2019).

[28]V. Y. Aleksandrov, K. Y. Arefyev, and M. A. Ilchenko, "Numerical and experimental investigation of non-stationary processes in the compact high enthalpy flow generators with gasdynamically ignition system," Izv. Ross. Akad. Nauk **6**, 96 (2014).

[29]B. Zhang, M. Shahsavari1, Z. Rao, R. Li, S. Yang, and B. Wang, "Effects of the fresh mixture temperature on thermoacoustic instabilities in a lean premixed swirl-stabilized combustor," Phys. Fluids **32**(4), 047101 (2020).

[30]R. I. Sujithand Vishnu and R. Unni, "Complex system approach to investigate and mitigate thermoacoustic instability in turbulent combustors," Phys. Fluids **32**(6), 061401 (2020).

[31]M. Shahsavari, M. Farshchi, S. R. Chakravarthy, A. Chakraborty, I. B. Aravind, and B. Wang, "Low swirl premixed methane-air flame dynamics under acoustic excitations," Phys. Fluids **31**(9), 095106 (2019).

[32]M. Shahsavari, B. Zhang, Z. Rao and S. Yang and B. Wang, "Contributions of hydrodynamic features of a swirling flow to thermoacoustic instabilities in a lean premixed swirl stabilized combustor," Phys. Fluids **31**(7), 075106 (2019).

[33]K. Deng, M. Wang, Z. Shen, Y. Hu, and Y. Zhong, "Effect of different acoustic parameters on NOx emissions of partially premixed flame," Appl. Sci. **9**(7), 1490 (2019).

[34]Z. D. Kravtsov, R. V. Tolstoguzov, L. M. Chikishev, and V. M. Dulin, "On formation of a stagnation zone in the flow between conical flame and flat obstacle," Thermophys. Aeromech. **25**(2), 317 (2018).

[35]A. I. Krikunova, "Premixed methane-air flame under alternate gravity," Acta Astronaut. **175**, 627 (2020).

[36]A. I. Krikunova, "M-shaped flame dynamics," Phys. Fluids **31**(12), 123607 (2019).

[37]A. I. Krikunova, "Effects of gravity on plane-symmetric rod-stabilized flame stabilization," High Temp. **57**(3), 430 (2019).

[38]S. Kheirkhaha and Ö. L. Gülder, "Turbulent premixed combustion in V-shaped flames: Characteristics of flame front," Phys. Fluids **25**(5), 055107 (2013).

[39]R. M. M. Mallens, B. O. Loijenga, L. P. H. De Goey, and P. J. M. Sonnemansb, "Numerical and experimental study of lean M–and V–shaped flames," Combust. Sci. Technol. **122**, 331 (1997).

[40]A. Tyagi, I. G. Boxx, S. J. Peluso, R. Shupp, and J. O'Connor, "Structure of flames in flame interaction zones," AIAA Aerospace Sciences Meeting (2018).

[41]M. Drkos, C. W. Leung, and C. S. Cheung, "Flame stability of rod stabilised premixed butane/air flames," J. Energy Inst. **82**(1), 1 (2009).

[42]I. Chterev and I. Boxx, "Effect of hydrogen enrichment on the dynamics of a lean technically premixed elevated pressure flame," Combust. Flame **225**, 149 (2021).

[43]M. Stöhr, K. Oberleithner, M. Sieber, Z. Yin, and W. Meier, "Experimental study of transient mechanisms of bistable flame shape transitions in a swirl combustor," J. Eng. Gas Turbines Power **140**(1), 011503 (2018).

[44]K. Oberleithner, M. Stöhr, S. H. Im, C. M. Arndt, and A. M. Steinberg, "Formation and flame–induced suppression of the precessing vortex core in a swirl combustor: experiments and linear stability analysis," Combust. Flame **162**(8), 3100 (2015).

[45]Z. Wang, X. Li, Z. Feng, and Z. Yang, "The role of precessing vortex core in two combustion regimes: Numerical simulation studies," J. Mech. Sci. Technol. **33**(1), 433 (2019).

[46]L. da Costa Ramos, F. Di Meglio, L. F. F. Da Silva, and V. Morgenthaler, "Reduced order model of laminar premixed inverted conical flames," AIAA Scitech 2020 Forum (2020), p. 0416.

[47]A. I. Krikunova, "M–shaped flame dynamics: Numerical simulation results," AIP Conf. Proc. **2304**, 020023 (2020).

[48]F. E. Hernandez Perez, H. G. Im, and A. E. Tingas, "Computational investigation of rod-stabilized laminar premixed hydrogen-methane-air flames," AIAA Scitech 2020 Forum (2020).
[49]L. Cifuentes, C. Dopazo, A. Sandeep, N. Chakraborty, and A. Kempf, "Analysis of flame curvature evolution in a turbulent premixed bluff body burner," Phys. Fluids **30**(9), 095101 (2018).
[50]B. R. Chowdhury and B. M. Cetegen, "Experimental study of the effects of free stream turbulence on characteristics and flame structure of bluff-body stabilized conical lean premixed flames," Combust. Flame **178**, 311 (2017).
[51]A. Karmarkar, A. Tyagi, S. Hemchandra, and J. O'Connor, "Impact of turbulence on the coherent flame dynamics in a bluff-body stabilized flame," Proc. Combust. Inst. **38**(2), 3067 (2020).
[52]M. Blanchard, T. Schuller, D. Sipp, and P. J. Schmid, "Response analysis of a laminar premixed M–flame to flow perturbations using a linearized compressible Navier–Stokes solver," Phys. Fluids **27**(4), 043602 (2015).
[53]T. Schuller, D. Durox, and S. Candel, "A unified model for the prediction of laminar flame transfer functions: comparisons between conical and V-flame dynamics," Combust. Flame **134**, 21 (2003).
[54]D. Durox, T. Schuller, N. Noiray, and S. Candel, "Experimental analysis of nonlinear flame transfer functions for different flame geometries," Proc. Combust. Inst. **32**, 1391 (2009).
[55]D. A. Lacoste, Y. Xiong, J. P. Moeck, S. H. Chung, W. L. Roberts, and M. S. Cha, "Transfer functions of laminar premixed flames subjected to forcing by acoustic waves, AC electric fields, and non-thermal plasma discharges," Proc. Combust. Inst. **36**(3), 4183 (2017).
[56]C. Foley, I. Chterev, B. Noble1, J. Seitzman, and T. Lieuwen, "Shear layer flame stabilization sensitivities in a swirling flow," Int. J. Spray Combust. Dyn. **9**(1), 3 (2017).
[57]R. L. Speth, "Fundamental studies in hydrogen-rich combustion: instability mechanisms and dynamic mode selection," Ph.D. thesis (Massachusetts Institute of Technology, 2010).
[58]H. M. Altay, R. L. Speth, D. E. Hudgins, and A. F. Ghoniem, "Flame-vortex interaction driven combustion dynamics in a backward-facing step combustor," Combust. Flame **156**(5), 1111 (2009).
[59]T. C. Lieuwen, *Unsteady Combustor Physics* (Cambridge University Press, New York, NY, 2012), p. 405.
[60]F. L. Ponta and H. Aref, "Strouhal-Reynolds Number Relationship for Vortex Streets," Phys. Rev. Lett. **9**(8), 084501 (2004).